The Astrophysical Journal Letters, 898:L36 (9pp), 2020 August 1 https://doi.org/10.3847/2041-8213/aba4b5

Observations of Small-scale Magnetic Reconnections within a Magnetic Flux Rope in Earth's Magnetosheath

Zhi Li[1,2]
[1] CAS Key Laboratory of Geospace Environment, Department of Geophysics and Planetary Science, University of Science and Technology of China, Hefei 230026, People's Republic of China; lorcd@mail.ustc.edu.cn
[2] CAS Center for Excellence in Comparative Planetology, Heifei, People's Republic of China
Received 2020 January 2; revised 2020 July 5; accepted 2020 July 10; published 2020 July 29

Abstract

The small-scale magnetic reconnection, which has been observed in turbulent plasma, is detected in the interior regions of an ion-scale flux rope in the magnetosheath. Reconnecting current sheets are configured with a nearly symmetric inflow boundary condition and a large guide field of six times the asymptotic field. The evidence of ongoing reconnection is consistent with the standard reconnection model, except no ion flow is detected. In this study, the electron shear flow near the current sheets allows the reconnections to occur. Strong dissipation with these reconnections indicate that electromagnetic energy can be effectively transformed into electron heating and kinetic energy. In particular, the small-scale reconnections do not result in an increase in high-energy electrons, but are responsible for an increase in electron flux over a lower energy range of 100–200 eV. Observations indicate that small-scale reconnection is very common and provides an important channel for energy dissipation in the magnetosheath plasma.

Unified Astronomy Thesaurus concepts: Space plasmas (1544)

1. Introduction

Magnetic reconnection is a fundamental physical mechanism that can impact the behavior of astrophysical and laboratory plasmas (Sonnerup 1981; Masuda et al. 1994; Mozer et al. 2002; Louarn et al. 2004; Gosling et al. 2005; Phan et al. 2007). It changes the magnetic topology and converts magnetic energy into particle thermal and kinetic energy. Most attention has been focused on large-scale reconnection between different plasmas (Paschmann et al. 1979; Øieroset et al. 2001; Gosling et al. 2005; Ren et al. 2005; Phan et al. 2006) during the past decades because it is commonly observed at the magnetosphere. In the standard reconnection model, this process takes place in a very small electron-scale diffusion region (Vasyliunas 1975; Burch et al. 2016). On the large scales, ions couple to the newly reconnected magnetic field lines and are ejected from the diffusion region as a bidirectional plasma jet at the ion-Alfvén speed (Paschmann et al. 1979; Phan et al. 2000; Gosling et al. 2005). Subsequently, numerous small-scale current sheets in turbulence plasma have been clarified from solar and laboratory measurements as well as simulations (Matthaeus & Montgomery 1980; Matthaeus & Lamkin 1986; Carbone et al. 1990; Simon et al. 2001; Cothran et al. 2003; Dmitruk & Matthaeus 2006).

It is well known that the magnetosheath region is a turbulent environment in the near-Earth space (Alexandrova et al. 2008; Huang et al. 2017; Bandyopadhyay et al. 2018). In this region, large-amplitude turbulence of density and magnetic field have been observed (Burgess et al. 2005), and thin current sheets are likely to occur. Many of these sheets are ion inertial length scales or smaller, and magnetic reconnection is easily initiated in thin current sheets (Pritchett 2001). Therefore, the magnetosheath should be an ideal place to study small-scale magnetic reconnection in turbulent plasma. As expected, small-scale magnetic reconnection associated with turbulence has recently been reported in Earth's magnetosheath (Retinò et al. 2007; Sundkvist et al. 2007; Vörös et al. 2017). In particular, as the oppositely directed electron outflow jets are detected by two spacecraft located on opposite sides of the X-line, electron-only magnetic reconnections have been identified in the magnetosheath (Phan et al. 2018). However, these reconnecting current sheets show the absence of ion jets, indicating the ions may not couple to the magnetic structures and any heating may only be transferred into the electrons. Although there are many small-scale reconnections in the magnetosheath, few energetic electrons have been reported in previous observations. Moreover, an outstanding question is to determine whether magnetic reconnection with a spatial size of less ion inertial lengths can generate in other plasma environments. In this Letter, for the first time, we present unambiguous in situ evidence of the existence of ongoing small-scale reconnections inside an ion-scale flux rope at Earth's magnetosheath. According to the preliminary analysis, such a situation should occur frequently in the near-space plasma environments.

2. Observations and Analysis

The Magnetospheric Multiscale (MMS) mission was launched on 2015 March 13 and was designed to perform a definitive exploration of magnetic reconnection at an electron scale (Burch et al. 2016). The Fluxgate Magnetometer (Russell et al. 2016; Torbert et al. 2016), the Fast Plasma Investigation (Pollock et al. 2016), and the Electric field Double Probe (Ergun et al. 2016; Lindqvist et al. 2016) provide comprehensive three-dimensional measurements of the related fields and particles involved in magnetic reconnection.

Figure 1 shows an overview of MMS2 observations from 05:57:02 UT and 05:57:20 UT on 2015 November 12. MMS was located at the magnetopause at a position of [11.3, 1.7, −1.3] Earth radius (R_E) in geocentric solar magnetospheric (GSM) coordinates. At this time four MMS spacecraft formed a small spacing (∼22 km) tetrahedron in space. Consequently, the data from all the spacecraft are very similar, so only data from MMS2 are presented here. All data are projected onto the

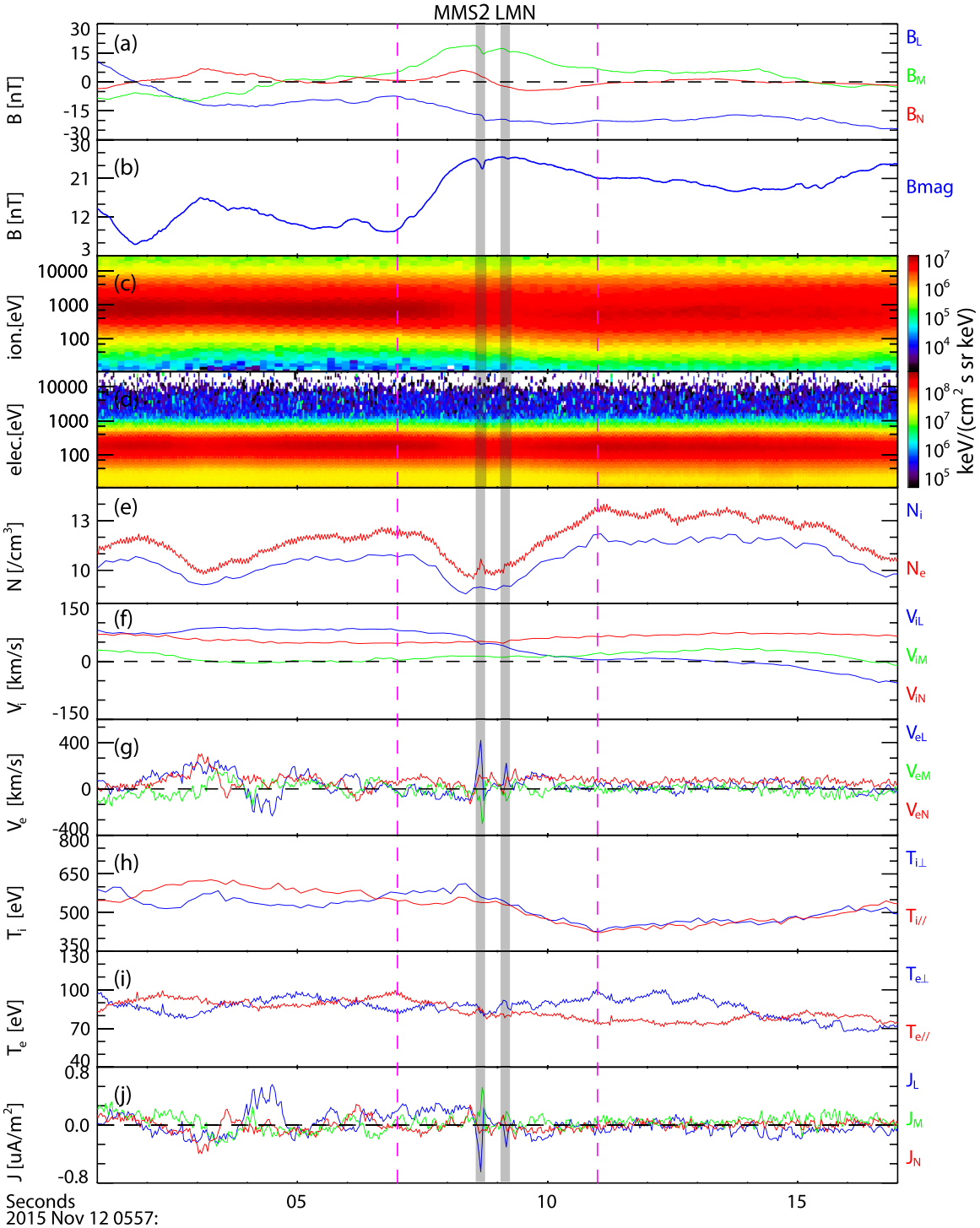

Figure 1. Overview of MMS2 observations in burst mode during 05:57:02 UT and 05:57:20 UT on 2015 November 12. (a) Magnetic field vector *LMN* coordinates, (b) magnetic field strength, (c)–(d) ion and electron energy spectra, (e) ion and electron number density, (f) ion bulk velocity components, (g) electron bulk velocity components, (h)–(i) ion and electron temperature, and (j) current density components. The vertical lines represent the boundaries of the flux rope.

local current sheet coordinate system (*LMN*), associated with the magnetopause crossing, which is derived by minimum variance analysis (MVA; Sonnerup & Scheible 1998) on the magnetic field from 05:56:58.0 UT to 05:57:12.0 UT. According to GSM, $N = [-0.95, 0.16, 0.25]$ is the boundary normal direction and almost opposite to the GSM-X axis, $L = [0.29, 0.27, 0.92]$ is basically the same as the the GSM-Z direction, and $M = [0.08, 0.95, -0.30]$ completes the right-hand system.

The spacecraft location was in the magnetosheath. The B_L (Figure 1(a)) component is stable and southward. Figure 1(e) shows ion and electron number density, which remained between 10 and 14 cm^{-3} during most of the time. Figures 1(h)–(i) display the parallel and perpendicular values of the ion and electron temperatures (T_i and T_e). As shown in Figure 1, background electron and ion temperatures are a few 10 eV and a few 100 eV, respectively. Figure 1(d) shows that the electron contains a low-energy component (<1 keV). All the features

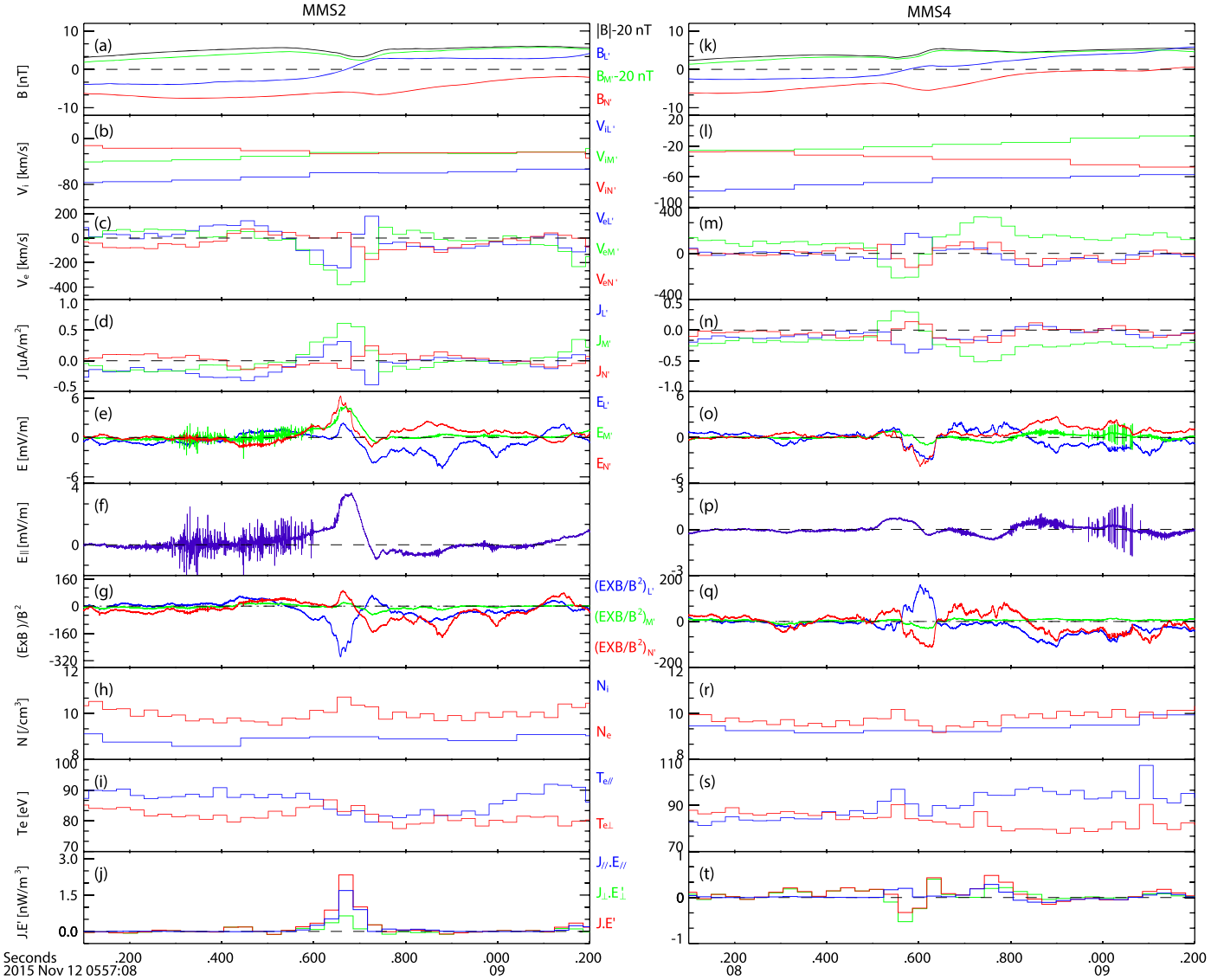

Figure 2. Simultaneous MMS2 and MMS4 detections of small-scale magnetic reconnection. The data for both spacecraft (MMS2, (a)–(j); MMS4, (k)–(t)) are shown in a common current sheet (*LMN*) coordinate system. (a), (k) Magnetic field, (b), (l) ion bulk velocity components, (c), (m) electron bulk velocity components, (d), (n) current density components, (f), (p) electric-field component parallel to the magnetic field, (g), (q) drift velocity, (h), (r) plasma density, (i), (s) electron temperature, and (j), (t) energy dissipation.

are consistent with those of the magnetosheath (Phan et al. 2007).

At 05:57:09 UT, a sharp reversal in the B_N component from $\sim+5$ to ~-5 nT is observed. The B_N reversal coincides with a maximum in the magnetic field magnitude in B_M and $|B|$ ($\sim$27 nT; Figures 1(a)–(b)), which is a standard characteristic of reconnected flux rope. The observations clearly show that MMS goes through a flux rope, since there is a simultaneous rotation in B_L indicating that the spacecraft are slightly off-center in their traversal of the flux rope. Spacecraft flux rope crossing time is 4 s, from when B_N started to increase from its magnetosheath value (at 05:57:07 UT) to when it changes to the original value (at 05:57:11 UT; vertical lines in Figure 1). Furthermore, plasma density presented a distinct decrease (from $\sim$12 to $\sim$9 cm^{-3}) within the flux rope (Figure 1(e)). The observed flux rope is embedded in a northward ion jet with a speed of about 80 km s^{-1} (Figure 1(f)), which is probably a reconnection outflow produced by a magnetopause X-line south of MMS.

A remarkable feature of this event is the occurrence of two minor magnetic field dips embedded within B_M and $|B|$ near the center of the flux rope (Figures 1(a)–(b)). A significant decrease is first observed at 05:57:08.7 UT when the magnetic field B_N has a positive value, and then another weak decrease is detected at 05:57:09.2 UT when B_N has a negative value (shaded areas in Figure 1). Both structures are associated with distinct electrons flow V_{eL} and V_{eM} (Figure 1(g)). As for the first dip, electron speed is 470 km s^{-1} and 270 km s^{-1} in L and M, respectively. As for the second one, the corresponding electron velocity is relatively small. This indicates that the current within the flux rope is filamentary, which has been reported in previous observations (Eastwood et al. 2016). In particular, electron shear flow is another feature near the current layers. Accompanying both the electron jets, the electron normal velocity V_{eN} reverses from the negative value to positive value. Here we mainly concentrate on the first magnetic structures in detail.

Figure 2 shows an expanded view of the crossing of the first magnetic structure. To understand the magnetic field fluctuation within the flux rope in detail, it is necessary to construct a reasonable coordinate system. All data are projected onto the $L'M'N'$, which is obtained by MVA on the magnetic field between 05:57:06.7 UT and 05:57:12.29 UT. According to the GSM, $M' = [-0.025,\ 0.523,\ -0.852]$, $N' = [0.986,\ 0.155,\ 0.067]$, and $L' = [0.167, -0.838, -0.520]$. $\boldsymbol{N}'$ is the boundary normal direction and nearly consistent with the GSM-X axis.

At 57:08.7 UT, a sharp reversal in the $B_{L'}$ component from -4 to 4 nT is observed. The $B_{L'}$ reversal coincided with a decrease in the magnetic field strength ($|B| = 23$ nT), and the perturbation of $B_{M'}$, which dominated the magnetic field (Figures 2(a)–(k)), all of which may be signatures of a reconnecting current sheet (Birn et al. 2001; Borg et al. 2005; Drake et al. 2008), and the following analysis will further confirm that reconnection is ongoing. The current sheet formed by the $B_{L'}$ reversal had approximately symmetric boundary conditions and the weaker reconnecting field, and the guide field $B_{M'}$ is dominated and about 6 times the reconnecting magnetic field.

Figure 2(c) shows the intense electrons bulk flow around the current sheet center at MMS2. Inside this current sheet, $V_{eM'}$ is always directed to the $-M'$ direction and the peak to $-400\ \mathrm{km\ s^{-1}}$. $V_{eL'}$ is negative, and peak value reaches $\sim -200\ \mathrm{km\ s^{-1}}$ near the current sheet center ($B_{L'} = 0$), and becomes weakly positive flows at both sides of the current sheet. The reversals of the electron flow in the L' direction are consistent with the expected results for a reconnection geometry. The electron jets in both the L' and M' directions are super-Alfvénic, for example, $V_{eM'} \sim 10\ V_A$ and $V_{eL'} \sim 7\ V_A$, where V_A is the ion-Alfvén speed ($V_{AiL'} \sim 29\ \mathrm{km\ s^{-1}}$) based on an electron number density of 9 per cubic centimeter and $B_{L'} = 4$ nT. The ion flow mostly is negative, and the bulk flow is less than $-70\ \mathrm{km\ s^{-1}}$ in this crossing. In other words, ions seemingly are not correlated with reconnection.

Coincident with the intense current layers, MMS4 simultaneously observed similarly strong out-of-plane electron flow with $V_{eM'} = -200\ \mathrm{km\ s^{-1}}$ and oppositely directed electron jets in the outflow direction, with $V_{eL'} = 200\ \mathrm{km\ s^{-1}}$, relative to an external electron flow in the L' direction of $V_{eL'} = -100\ \mathrm{km\ s^{-1}}$ (Figure 2(m)). The speed of these electron jets is roughly 7 times the asymptotic ion-Alfvén speed. As expected for a reconnection geometry with inflow from both sides, the changes in $V_{eL'}$ for MMS4 are exactly the opposite of that of MMS2. Definitive evidence for reconnection would be the simultaneous detection of oppositely directed plasma outflow jets by two spacecraft located on opposite sides of the X-line (Phan et al. 2000, 2018). An expected result here indicates that the reconnection site (or X-line) must have been between MMS2 and MMS4. Furthermore, accompanying $B_{L'}$ reversal, a bipolar perturbation in $B_{M'}$ from positive to negative is observed by MMS2, while a bipolar perturbation in $B_{M'}$ from negative to positive is observed by MMS4 (Figures 3(d)–(e)). This is consistent with the Hall magnetic signatures observed by the two spacecraft in the opposite outflow region. Accordingly, the location of the four spacecraft at this time is shown in Figure 3(a) with the projection of the tetrahedron in the plane $L'N'$. Based on the observations above, a schematic illustration for the reconnecting event is displayed in Figure 3(c).

The measurements of the electron outflow jets at MMS2 are further supported by the higher-resolution measurements of the L' component of the drift velocity $(\boldsymbol{E} \times \boldsymbol{B})/B^2$ (where $\boldsymbol{E}$ is the electric field and $\boldsymbol{B}$ is the magnetic field), which is negative at MMS2 (Figure 2(g)). The related drift velocity of MMS4 is positive (Figure 2(q)), all of which are similar to the observed electron velocity in the L direction. These $(\boldsymbol{E} \times \boldsymbol{B})/B^2_{L'}$ outflows are predominantly perpendicular to the magnetic field, owing to the dominant $B_{M'}$ (Figures 2(a), (k)) together with the large $E_{N'}$ (Figures 2(e), (o)) driving the outflows. There is no evidence for ion jets at the ion-Alfvén speed (Figures 2(b), (l)) within the current sheets. The reason for the absence of the ion jet in this event is still unclear. One potential reason is due to the lack of space and time for ions to couple magnetic fields (Phan et al. 2018). Moreover, $E_{N'}$ is opposite within the reconnection sheet at the two spacecraft (Figures 2(e), (o)), which is consistent with the feature of electron-only reconnection (Phan et al. 2018). The features of the second thin current sheet are similar to the first one at MMS2, and a detailed analysis is shown in the Appendix.

The current density can be estimated directly according to the formula $\boldsymbol{J} = n_e e(\boldsymbol{V}_i - \boldsymbol{V}_e)$, where n_e is the electron number density and e is the elementary coulomb charge, respectively. Inside the first current sheet, both MMS2 and MMS4 observed mainly out-of-plane electron current $J_{M'}$ (Figures 2(d), (n)). The current densities associated with the reversal of magnetic field component $B_{L'}$ peak at $0.7\ \mu\mathrm{A\ m^{-2}}$ and $0.4\ \mu\mathrm{A\ m^{-2}}$, respectively. Similar trends to electron velocities mean that the current is mainly carried by electrons.

Multispacecraft timing analysis (Schwartz 1998; Dunlop et al. 2002) indicates that the current sheet moves sunward in the current sheet normal direction (where $\boldsymbol{N} = L'M'N'$ (0.3747, 0.0649, 0.9249)) with a speed of $52\ \mathrm{km\ s^{-1}}$. The derived normal direction is identical with the $\boldsymbol{N}'$ calculated from minimum variance analysis. The duration for the current sheet is ~0.18 s (~05:57:08.6 and ~05:57:08.78 UT). Thus, the thickness of the current sheet is calculated to be $52\ \mathrm{km\ s^{-1}} \times 0.18\ \mathrm{s} = 9.36\ \mathrm{km}$ $\sim 5.5\ d_e$, where d_e is the electron inertial length. In the turbulent magnetosheath, similar intense small-scale current sheets are favorable sites for electron-only reconnection (Stawarz et al. 2019). Four-spacecraft timing analysis can also be applied to gain quantitative information about the orientation and motion of the flux rope. In the case of a cylindrically symmetric flux rope, it can be shown that the times at which each spacecraft observes the peak field strength define a plane that is perpendicular to the tetrahedron direction of motion and contains the axis of the flux rope. The flux rope is found to be moving at $v \sim 43.5\ \mathrm{km\ s^{-1}}$ along $\boldsymbol{n} = (0.83, 0.26, 0.49)$ GSM relative to MMS. The velocity of the flux rope is found to be mainly in the x–z plane, indicating that the axis of the structure is nearly in the y direction. This orientation is also consistent with the result calculated by MVA also shown previously. As mentioned above, the flux rope crossing time is 4 s during 05:57:07 UT and 05:57:11 UT. This corresponds to a crossing distance of 174 km based on the normal speed of $43.5\ \mathrm{km\ s^{-1}}$ of the flux rope, or $2.26\ d_i$. This indicates that the spacecraft are observed an ion-scale flux rope. As previously analyzed, the spacecraft are slightly off-center when crossing the flux rope. This means that any estimate of the flux rope size is a lower bound.

MMS2 observed well-defined parallel electric fields (Figure 2(f)), which indicated the invalidation of the ideal electron frozen-in condition $(\boldsymbol{E}' = \boldsymbol{E} + \boldsymbol{V}_e \times \boldsymbol{B} = 0)$. The

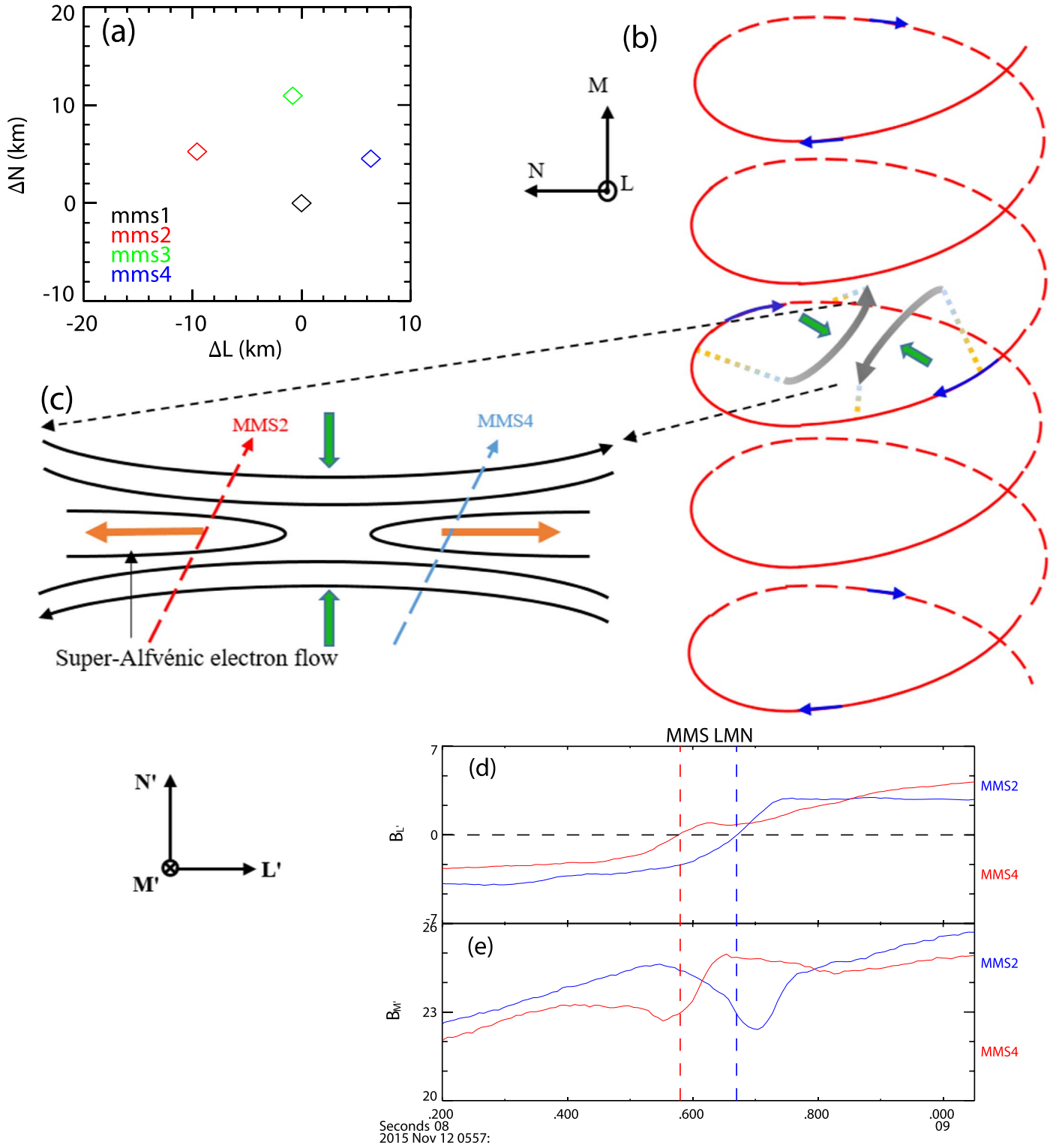

Figure 3. Schematics of MMS orbits relative to the flux rope and magnetic reconnection. (a) MMS tetrahedron configuration, (b) a 3D schematic of field lines of the flux rope, (c) a zoomed-in 2D view of the electro-scale reconnection, (d) magnetic field B_L observed by MMS2 and MMS4, and (e) magnetic field B_M observed by MMS2 and MMS4. The green arrows in (b) and (c) indicate the electron inflow, and the orange arrows indicate super-Alfvénic electron outflow in (c).

electron dissipation measure ($\boldsymbol{J}\cdot\boldsymbol{E}'$) is calculated in Figure 2(j) based on current densities and electric field in the electron frame. $\boldsymbol{J}\cdot\boldsymbol{E}'$ is positive within the current sheet and is close to zero when MMS crossed outside the exhaust region. The electric field structure is parallel to the background magnetic field at MMS2. The dissipation is positive and basically all dominated by $J_{||}E_{||}$. The energy dissipation is mainly contributed by the parallel electric field within/near the electron diffusion region (EDR) with a large guide field (Genestreti et al. 2017; Zhou et al. 2017). However, the energy dissipation of the current sheet observed by MMS4 is fluctuating and insignificant on average (Figure 2(t)). And

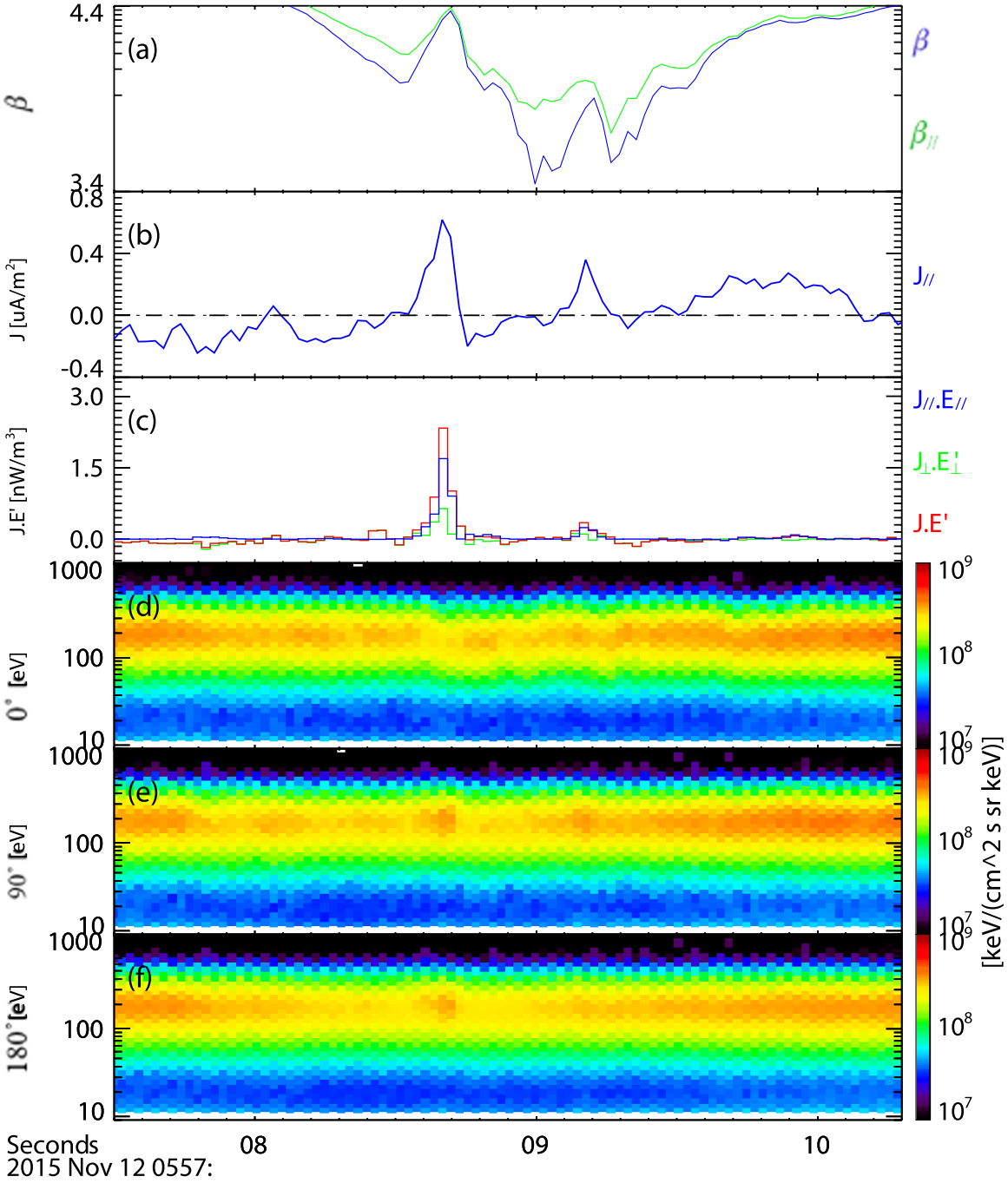

Figure 4. Electrons characteristics are associated with two small-scale reconnections. (a) β value, (b) parallel current density, (c) energy dissipation, and (d)–(f) spectrograms of the electron differential energy flux.

parallel electric fields are not obvious (Figure 2(p)). The origin of the difference in energy dissipation and the electric field in opposite outflow regions is currently unclear.

The energy conversion can be estimated according to Phan et al. (2018) method. Here, one-fifth of the available magnetic energy per particle (one-fifth of 8 eV) in the inflow regions ($m_e V_{AeL'}^2$), where m_e is the electron mass and $V_{AeL'} \sim 1193\,\mathrm{km\,s^{-1}}$ is the electron-Alfvén speed, goes into kinetic energy associated with $V_{eM'}$ and $V_{eL'}$, which are 34% and 25% of $V_{AeL'}$, respectively. The remaining energy (~6.4 eV) converted entirely into the electron heating, resulting in an enhancement in electron temperature of $6.4\,\mathrm{eV} \times (\gamma - 1)/\gamma \sim 2.6\,\mathrm{eV}$ in the reconnecting current sheet, where $\gamma = 5/3$, is the ratio of the specific heats. This is a small temperature increase, which is consistent with previous observations (Phan et al. 2018) and would not be evident in the data (Figures 2(i), (s)).

Although it is known that very little energy is converted to electron heat in such current sheets, the specific heating process is still unknown. The effect of small-scale magnetic field reconnection on electrons can be seen in Figure 4. The electron plasma β (Figure 4(a)) becomes very large, reaching values of up to 4.4 and 3.5 in the center of the first and second current sheets, respectively, which means that the available magnetic energy is comparable to the electron thermal energy. It can also

be found that β peaks correlate well with enhancements of the parallel current density and peaks of energy dissipation (Figures 4(b)–(c)). The spectrogram of the differential energy flux parallel, perpendicular and antiparallel to the local magnetic field direction, are shown in panels (g)–(i), respectively. The spectrogram of the differential energy flux shows that the thermal energy of the electrons, which is approximately the energy corresponding to the maximum flux, increases within the current sheet (about 05:57:08.7 and 05:57:09.2 UT). For both thin current sheets at MMS2, such electron flux enhancement appears over a lower energy range of 100–200 eV in perpendicular and antiparallel directions, which is consistent with the exhibition of electron energy dissipation (Figure 2(s)). However, it is worthwhile to note that the electron temperature has not increased significantly when the reconnection events occurred at current sheets that are approaching electron-scale thicknesses, while the electron densities in both thin current sheets have increased significantly with respect to both sides. It appears that the enhanced electron energy flux is mainly associated with enhanced density, and may be related to slight electron heating. To quantitatively assess the importance of reconnection in dissipating energy in small systems, it is necessary to investigate the basic properties of small-scale reconnection in theory and observation.

3. Summary and Conclusion

Here we report the simultaneous multispacecraft detection of oppositely directed super-ion-Alfvénic electron jets, parallel electric fields, and magnetic-to-particle energy conversion in an electron-scale current sheet inside an ion-scale flux rope, providing direct evidence for small-scale reconnection in the flux rope. The reconnection layer, with a thickness $\sim 5.5\, d_e$, is defined by symmetric boundary conditions in the presence of a strong guide field. Current sheets inside the flux ropes have previously been reported but were not resolved due to limitations of previous plasma instruments (Hasegawa et al. 2010; Øieroset et al. 2011, 2014). One possibility is that the reconnection at the flux rope center is generated between field lines carried by the converging jets (Øieroset et al. 2016). The ions do not have a response to the reconnection process in the thin current sheet, and the electron jet reversals in the N direction coincide with both intense currents at MMS2, which indicates that the electron shear flow forms near the current sheets. Velocity field shear may lead to the onset of the Kelvin–Helmholtz instability (Chandrasekhar 1961; Miura & Pritchett 1982) that causes magnetic field lines to reconnect (Dungey 1961; Li et al. 2016). The evidence suggests that the small-scale reconnection is ubiquitous in the magnetosphere, even in the flux rope.

The source of high-energy particles in the inner magnetosphere has been a long-standing question. Particle acceleration by magnetic reconnection has been found to occur up to hundreds of keV in the magnetotail region (Øieroset et al. 2002), but rarely reported in the magnetosheath. If the energetic electrons are produced by small-scale reconnection, then particle accelerated to high energy (>10 keV) should be common in the magnetosheath that contained a large number small-scale current (Retinò et al. 2007; Sundkvist et al. 2007), whereas the speculation is not consistent with previous observations. Compared to our results, observations clearly show that reconnection acts as an electromagnetic energy conversion channel as $\boldsymbol{J}\cdot\boldsymbol{E}' > 0$, especially we certify that the thermal energy of the electrons is enhanced at the energy 100–200 eV. The small-scale reconnection does not correspond to the increase of high-energy ions and electrons (Figures 4(d)–(f)). Our finding supports the clear view that small-scale reconnection has a general role in dissipating the energy in space and astrophysical environment. However, more properties of these reconnections will be needed to be investigated theoretically and observationally, for example, how these reconnections happen inside the flux rope is still an intriguing question.

We thank the entire MMS team and MMS Science Data Center for providing the high-quality data for this study (https://lasp.colorado.edu/mms/sdc/public/).

Appendix

Figure A1 shows an overview of the crossing of the second current sheet observed by MMS2 during the 05:57:08.8–05:57:09.5 UT. The data are given in local current sheet coordinates (LMN) where $L = (0.141, -0.909, -0.391)$, $M = (0.014, 0.397, -0.918)$, and $N = (0.989, 0.124, 0.068)$. N is nearly consistent with the normal direction of the first current sheet as mentioned above. The B_L component reverses from -1 to 1 nT and is observed at about 57:09.19 UT. The thickness of the current sheet is calculated to be $52\ \mathrm{km\ s^{-1}} \times 0.13\ \mathrm{s} \approx 6.76\ \mathrm{km} \sim 4d_e$, where d_e is the electron inertial length.

V_{eL} is negative ($\sim -60\ \mathrm{km\ s^{-1}}$) near the current sheet center. V_{eM} is directed to the $-M$ direction and the peak to $-280\ \mathrm{km\ s^{-1}}$. The electron jets in both the L and M directions are super-Alfvénic, for example, $V_{eM} \sim 27V_{\mathrm{A}}$ and $V_{eL} \sim 8V_{\mathrm{A}}$, where V_{A} is the ion-Alfvén speed ($V_{\mathrm{A}iL} \sim 7.3\ \mathrm{km\ s^{-1}}$) based on an electron number density of 9 per cubic centimeter and $B_L = 1$ nT.

MMS2 observed well-defined parallel electric fields (Figure A1(f)). The electron dissipation measure ($J \cdot E'$) was calculated in Figure A1(i) based on current densities and the electric field in the electron frame. $J \cdot E'$ was positive within the current sheet and was close to zero when MMS crossed outside the exhaust region.

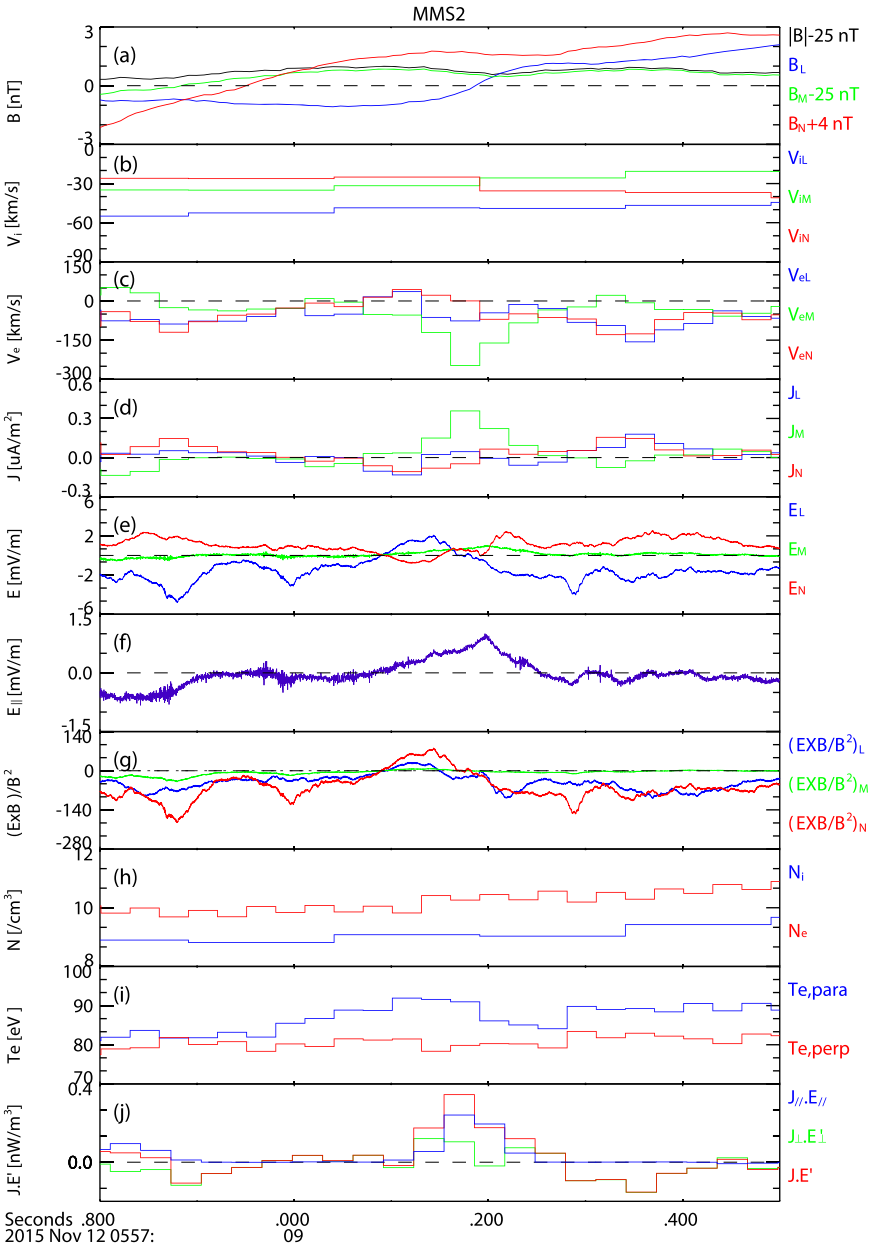

Figure A1. Overview of the second current sheet observed by MMS2 in the burst mode during 05:57:08.8–05:57:09.5 UT on 2015 November 12.

References

Alexandrova, O., Lacombe, C., & Mangeney, A. 2008, AnGeo, 26, 3585
Bandyopadhyay, R., Chasapis, A., Chhiber, R., et al. 2018, ApJ, 866, 106
Birn, J., Drake, J. F., Shay, M. A., et al. 2001, JGR, 106, 3715
Borg, A. L., Øieroset, M., Phan, T. D., et al. 2005, GeoRL, 32, L19105
Burch, J. L., Torbert, R. B., Phan, T. D., et al. 2016, Sci, 352, aaf2939
Burgess, D., Lucek, E. A., Scholer, M., et al. 2005, SSRv, 118, 205
Carbone, V., Veltri, P., & Mangeney, A. 1990, PhFlA, 2, 1487
Chandrasekhar, S. 1961, Hydrodynamic and Hydromagnetic Stability (New York: Oxford Univ. Press)
Cothran, C. D., Landreman, M., Matthaeus, W. H., & Brown, M. R. 2003, GeoRL, 30, 1213
Dmitruk, P., & Matthaeus, W. H. 2006, PhPl, 13, 042307
Drake, J. F., Shay, M. A., & Swisdak, M. 2008, PhPl, 15, 042306
Dungey, J. W. 1961, PhRvL, 6, 47
Dunlop, M. W., Balogh, A., Glassmeier, K.-H., & Robert, P. 2002, JGRA, 107, 1384
Eastwood, J. P., Phan, T. D., Cassak, P. A., et al. 2016, GeoRL, 43, 4716
Ergun, R. E., Tucker, S., Westfall, J., et al. 2016, SSRv, 199, 167
Genestreti, K. J., Burch, J. L., Cassak, P. A., et al. 2017, JGRA, 122, 11342
Gosling, J. T., Skoug, R. M., McComas, D. J., & Smith, C. W. 2005, JGRA, 110, A01107
Hasegawa, H., Wang, J., Dunlop, M. W., et al. 2010, GeoRL, 37, L16101
Huang, S. Y., Hadid, L. Z., Sahraoui, F., et al. 2017, ApJL, 836, L10
Li, W., André, M., Khotyaintsev, Y. V., et al. 2016, GeoRL, 43, 5635
Lindqvist, P. A., Olsson, G., Torbert, R. B., et al. 2016, SSRv, 199, 137
Louarn, P., Fedorov, A., Budnik, E., et al. 2004, GeoRL, 31, L19805
Masuda, S., Kosugi, T., Hara, H., Tsuneta, S., & Ogawara, Y. 1994, Natur, 371, 495
Matthaeus, W. H., & Lamkin, S. L. 1986, PhFl, 29, 2513
Matthaeus, W. H., & Montgomery, D. 1980, NYASA, 357, 203
Miura, A., & Pritchett, P. L. 1982, JGR, 87, 7431
Mozer, F. S., Bale, S. D., & Phan, T. D. 2002, PhRvL, 89, 015002
Øieroset, M., Lin, R. P., Phan, T. D., Larson, D. E., & Bale, S. D. 2002, PhRvL, 89, 195001
Øieroset, M., Phan, T. D., Eastwood, J. P., et al. 2011, PhRvL, 107, 165007
Øieroset, M., Phan, T. D., Fujimoto, M., Lin, R. P., & Lepping, R. P. 2001, Natur, 412, 414
Øieroset, M., Phan, T. D., Haggerty, C., et al. 2016, GeoRL, 43, 5536

Øieroset, M., Sundkvist, D., Chaston, C. C., et al. 2014, JGRA, 119, 6256
Paschmann, G., Sonnerup, B., Papamastorakis, I., et al. 1979, Natur, 282, 243
Phan, T. D., Drake, J. F., Shay, M. A., Mozer, F. S., & Eastwood, J. P. 2007, PhRvL, 99, 255002
Phan, T. D., Eastwood, J. P., Shay, M. A., et al. 2018, Natur, 557, 202
Phan, T. D., Gosling, J. T., Davis, M. S., et al. 2006, Natur, 439, 175
Phan, T. D., Kistler, L. M., Klecker, B., et al. 2000, Natur, 404, 848
Pollock, C. J., Moore, T., Jacques, A., et al. 2016, SSRv, 199, 331
Pritchett, P. L. 2001, JGR, 106, 25961
Ren, Y., Yamada, M., Gerhardt, S., et al. 2005, PhRvL, 95, 55003
Retinò, A., Sundkvist, D., Vaivads, A., et al. 2007, NatPh, 3, 236
Russell, C. T., Anderson, B. J., Baumjohann, W., et al. 2016, SSRv, 199, 189
Schwartz, S. J. 1998, in Analysis Methods for Multi-Spacecraft Data, ed. G. Paschmann & P. W. Daly (Noordwijk: ESA), 249
Simon, G. W., Title, A. M., & Weiss, N. O. 2001, ApJ, 561, 427
Sonnerup, B. U. 1981, JGR, 86, 10049
Sonnerup, B. U. Ő., & Scheible, M. 1998, in Analysis Methods for Multi-Spacecraft data, ed. G. Paschmann & P. W. Daly (Noordwijk: ESA), 185
Stawarz, J. E., Eastwood, J. P., Phan, T. D., et al. 2019, ApJL, 877, L37
Sundkvist, D., Retinò, A., Vaivads, A., & Bale, S. D. 2007, PhRvL, 99, 25004
Torbert, R. B., Russell, C. T., Magnes, W., et al. 2016, SSRv, 199, 105
Vasyliunas, V. M. 1975, RvGSP, 13, 303
Vörös, Z., Yordanova, E., Varsani, A., et al. 2017, JGRA, 122, 11442
Zhou, M., Ashour-Abdalla, M., Deng, X., et al. 2017, JGRA, 122, 9513